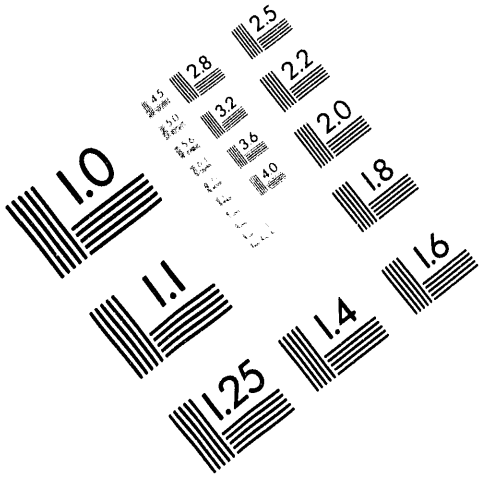

Association for Information and Image Management

1100 Wayne Avenue, Suite 1100
Silver Spring, Maryland 20910

301/587-8202

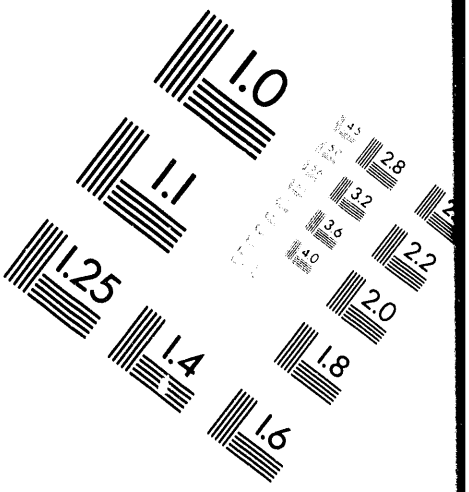

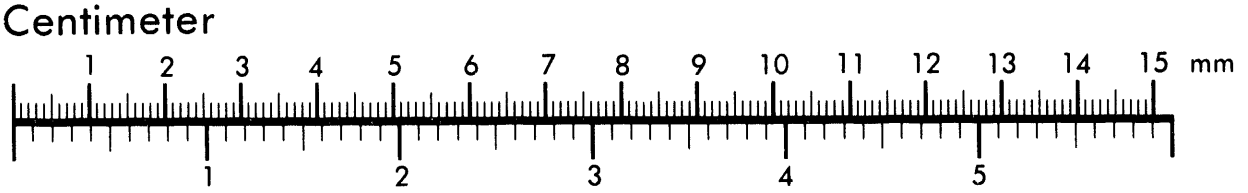

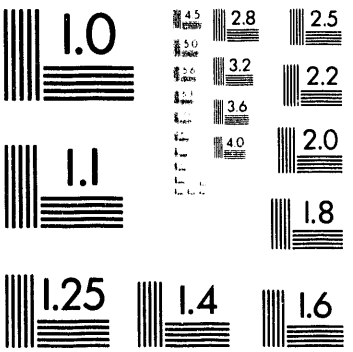

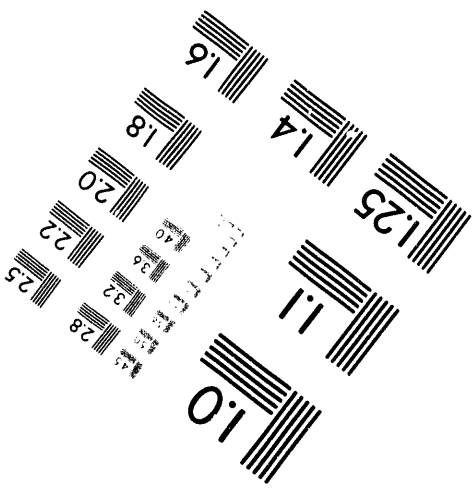

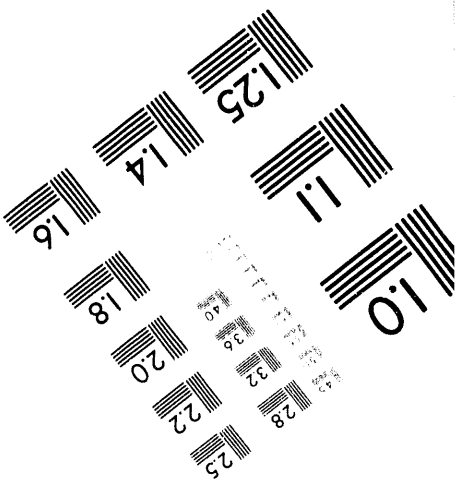

MANUFACTURED TO AIIM STANDARDS
BY APPLIED IMAGE, INC.

1 of 1

LA-UR- 94-1811

Title: CHANNEL PROBE MEASUREMENTS FOR THE AMERICAN SECTOR CLUTTER EXPERIMENT, JANUARY, 1994

Author(s): T. Joseph Fitzgerald

Submitted to: Neil B. Myers
Rome Air Development Center
RADC/EECP
Hanscom AFB, MA 01731

MASTER

Los Alamos
NATIONAL LABORATORY

Form No. 836 R5
ST 2629 10/91

Channel Probe Measurements for the American Sector Clutter Experiment, January, 1994

T. Joseph Fitzgerald
Los Alamos National Laboratory, Los Alamos, New Mexico 87545

May 20, 1994

Contents

Abstract 3

1 Introduction. 4

2 Experiment. 4
- 2.1 CW System . . . 5
- 2.2 Oblique Ionogram System . . . 7
- 2.3 Channel Probe System . . . 8
- 2.4 AVA One-Way Propagation . . . 10
- 2.5 Antenna Geometry . . . 10
- 2.6 Problems . . . 10

3 Results. 12
- 3.1 Oblique Ionograms . . . 12
- 3.2 CW Doppler Spectra . . . 12
- 3.3 CW Spatial Coherence . . . 15
- 3.4 Channel Probe Time Delay . . . 17
- 3.5 Channel Probe Doppler Spectra . . . 17
- 3.6 Channel Probe Spatial Coherence . . . 19
- 3.7 AVA Time Delay . . . 19
- 3.8 AVA Doppler Spectra . . . 21

4 Conclusions. 23

5 Acknowledgement 23

6 References 23

Abstract

The ionospheric phenomenon called Equatorial Spread F encompasses a variety of effects associated with plasma irregularities occurring in the post-sunset and nighttime ionosphere near the magnetic equator. These irregularities can seriously degrade the performance of systems which involve either of necessity or inadvertently radio propagation through the equatorial ionosphere. One such system is Over-the-Horizon (OTH) radars which operate in the high-frequency (hf) band and use ionospheric reflection for forward and backscatter propagation to ranges of thousands of kilometers. When such radars are directed towards the equator, Spread F irregularities can cause scintillation effects which may be aliased into the ranges of interest and have the effect of causing excess clutter in which targets may be hidden. In January, 1994 Los Alamos participated in a campaign to measure Spread F effects on OTH propagation from the United States looking towards South America in conjunction with local diagnostics in Peru. During the campaign Los Alamos fielded a 1600 km bistatic path between Piura, Peru, and Arequipa, Peru; the one-hop reflection region for this path was near the magnetic equator. We obtained four types of measurements: an oblique ionogram between Piura and Arequipa every three minutes; Doppler spread and spatial correlation for a single frequency cw path between Piura and Arequipa; Doppler spread, time-delay spread, and spatial coherence for a 10 kHz bandwidth path between Piura and Arequipa; and Doppler spread and time-delay spread for the one-way path between the AVA radar in New York and Arequipa, Peru. This report describes the diagnostic experiments that we carried out and gives a brief description of some of the data we obtained.

1 Introduction.

The ionospheric phenomenon called Equatorial Spread F encompasses a variety of effects associated with plasma irregularities occurring in the post-sunset and nighttime ionosphere near the magnetic equator. These irregularities can seriously degrade the performance of Over-the-Horizon (OTH) radars directed towards the equator by inducing range-aliased clutter in which targets may be hidden. In January, 1994 Los Alamos participated in a campaign to measure Spread F effects on OTH propagation from the United States looking towards South America in conjunction with local diagnostics in Peru. During the campaign Los Alamos fielded a 1600 km bistatic path between Piura, Peru, and Arequipa, Peru; the one-hop reflection region for this path was near the magnetic equator. We obtained four types of measurements: an oblique ionogram between Piura and Arequipa every three minutes; Doppler spread and spatial correlation for a single frequency cw path between Piura and Arequipa; Doppler spread, time-delay spread, and spatial coherence for a 10 kHz bandwidth path between Piura and Arequipa; and Doppler spread and time-delay spread for the one-way path between the AVA radar in New York and Arequipa, Peru. This report describes the diagnostic experiments that we carried out and gives a brief description of some of the data we obtained.

2 Experiment.

Our transmitter site was located at the University of Piura, in the city of Piura in northern Peru (5° 30' S, 81° 0' W); our receiver site was at the Peruvian Air Force Base, in the city of Arequipa in southern Peru (16° 20' S, 71° 34' W, 2630 m). The great circle distance between the sites was 1600 km while the azimuth at mid-path was $-40°$. The mid-path was 125 km northeast of Jicamarca (11.9° S, 77° W). The great circle distance between the AVA transmitter (43° 47' N, 75° 5' W) and the Arequipa receiver site was 6700 km; the azimuth at the receive site was $-3°$.

We attempted four types of propagation measurements during the experiment. The first was an oblique ionogram between Piura and Arequipa to obtain time delay spread versus frequency. We obtained this data over frequencies from 4 to 20 MHz every 180 s. Most of the time the maximum-usable-frequency (muf) was less than 20 MHz but at some times our oblique ionogram did not reach the muf. For the second measurement we used a single-frequency cw transmission between Piura and Arequipa to determine Doppler spread and spatial correlation over four antennas spaced across the path. This measurement folds all possible propagation modes into the data but it is usually possible to separate multihop propagation because of a different power level and Doppler shift. The third measurement was a channel probe between Piura and Arequipa for which we used an fmcw chirp with a sweep rate of 100 kHz/s and a repetition frequency of 10 Hz to obtain to obtain 2.5 ms of time delay information with a resolution of .1 ms and an unambiguous Doppler of ± 5 Hz. We collected this data from three of the most closely spaced antennas. For the fourth measurement, we tuned one element of our channel probe system to the AVA radar transmission from New York. That radar broadcasted with the same parameters as

Day (EST)	Time (EST)	Probe	AVA	Jicamarca	Digisonde	Spread F (EST)
Jan 10	2000–2400	Yes	Yes	No	No	2030–2400
Jan 11	1830–2400	Yes	Yes	Yes	Yes	2300–2400
Jan 12	1830–2400	Yes	Yes	<2145	Yes	2030–2400
Jan 13	1830–2400	Yes	Yes	Yes	Yes	2145–2400
Jan 14	1830–2400	Yes	Yes	Yes	Yes	1925–2400

Table 1: Time schedule for the data collection during the channel probe experiment.

the channel probe but at a different frequency. We thus collected time delay and Doppler for the 6700 km AVA-Arequipa path. We could hear the oblique sounder from AVA but we were not able to synchronize our oblique ionogram system to it so we did not obtain any ionogram information for the AVA-Arequipa path. We did not collect data from the transmissions of either the ROTHR or ECRS radars.

We collected data over a period of five nights concentrated on the post-sunset period for which we expected the highest probability of spread F. The Jicamarca radar operated on all but the first night although no data was acquired between 2145 and 2400, Jan. 12 (EST). The Digisonde at Jicamarca also obtained data on all but the first night. The AVA radar operated on all of the nights. Spread F was strong on the first and last nights; it was weak on the second and fourth nights and intermediate on the third night. We collected data from four antennas for both the channel probe and AVA on the first and second nights although most of these channels had a low signal to noise ratio. The other nights we collected only one antenna of AVA and three antennas of channel probe but with considerably improved performance. Table 1 lists the time schedule of the experiment.

2.1 CW System

We collected four channels of cw data on the Piura to Arequipa path at a single frequency which was offset from the channel probe frequency 30 kHz. Each channel represented one of the four spatially separated antennas. The transmitter system consisted of a HP synthesizer feeding a power amplifier. The synthesizer was locked to the 10 MHz reference from the GPS receiver. The 300 W output of the amplifier was fed to a tilted delta antenna directed towards Piura. The received signal, after amplification at the antenna, was brought in by cable to a splitter from which one output was directed to a Racal receiver for cw processing while another output was directed to the channel probe system. The receiver reference was locked to the 1 MHz output from a Rubidium clock. The receivers were operated with a 50 Hz BFO offset and a nominal bandwidth of 100 Hz. The output audio signal was sampled at a 500 Hz rate by the digitizer giving a 250 Hz Nyquist frequency. Figure 1 shows a block diagram of the transmit and receive portions of the cw system.

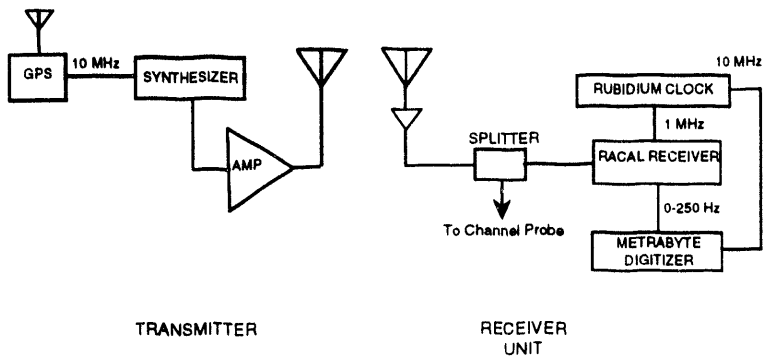

Figure 1: Diagram of the continuous-wave (cw) transmitter and receiver system.

Table 2 lists the operational cw frequencies for the data collection periods; during the one hour time period, 2200-2300 EST on Jan. 14, we changed frequencies in 1 MHz steps every 15 minutes.

Day (EST)	Time (EST)					
	1800	1900	2000	2100	2200	2300
Jan 10			10.87	9.37	9.37	9.37
Jan 11	11.37	10.87	10.87	9.37	9.37	9.37
Jan 12	11.37	10.87	10.87	9.37	9.37	9.37
Jan 13	11.37	10.87	10.87	12.87	12.87	12.87
Jan 14	13.37	12.87	12.87	multi	10.87	10.87

Table 2: CW frequency in MHz.

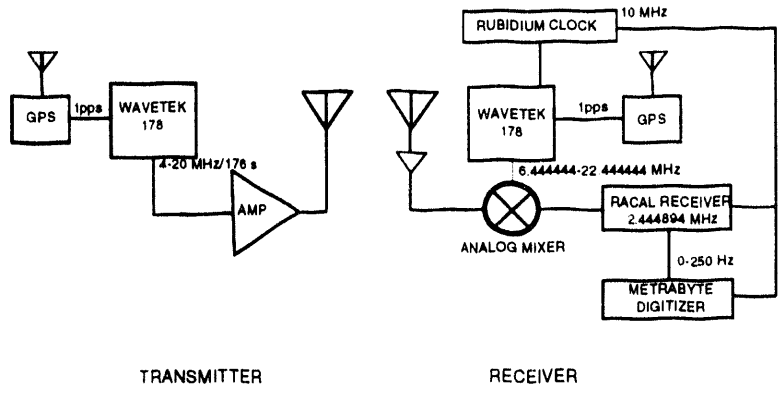

Figure 2: Diagram of the oblique ionogram transmitter and receiver system.

2.2 Oblique Ionogram System

Our oblique ionogram system is similar to the commercially available Barry sounders in that it uses the fmcw radar technique of measuring time delay by measuring the frequency offset of a received linear sweep relative to the transmitted sweep. Figure 2 shows a block diagram of the transmit and receive portions of the cw system. At the transmitter end we use a Wavetek 178 synthesizer to generate an rf waveform which linearly sweeps in frequency over the range of interest. For the experiment we used 4 to 20 MHz. The start of the sweep is triggered by the 1 pps output of a GPS receiver. If we set the sweep duration for 176 s then after three seconds dead time the synthesizer is ready for the the next trigger at 180 s after the first so the sweep repeats every three minutes. The sweep rate was 90.91 kHz/s. The output of the synthesizer was fed into a broad-band amplifier to give an output power of 300 W into a end-fired delta antenna. The reference frequency of the synthesizer was locked to the 10 MHz output of the GPS receiver.

At the receive end, we mix the amplified rf from the antenna with the output of another Wavetek 178 synthesizer. We set the sweep duration to 176 s and trigger on the identical second using the 1 pps from a GPS receiver. We used a Rubidium clock for the reference frequency for the synthesizer. However, we offset the frequency of the Wavetek by 2.444444 MHz from the transmit end so that the output of the mixer can be fed into a Racal receiver for detection. We actually tuned the receiver to a frequency of 2.444894 MHz to compensate for most of the propagation delay. The receiver is operated in cw mode with 0 BFO offset and about 250 Hz bandwidth. There appears to be no significant time delay in the mixer, so that the frequency output of the receiver plus the 450 Hz offset can be divided by 90.91 kHz to get the time delay in seconds.

We sampled the audio output at a 500 Hz rate giving an unambiguous time delay range of 2.75 ms. The rolloff of the audio filter is relative slow so that multihop does appear. We analyze the data by doing a short term power spectrum, for example, 1024 samples, which gives a frequency resolution of about .5 Hz or an effective bandwidth of 186 kHz. Errors in the trigger from the GPS clock, which are supposed to be about 1 μs, affect the repeatability

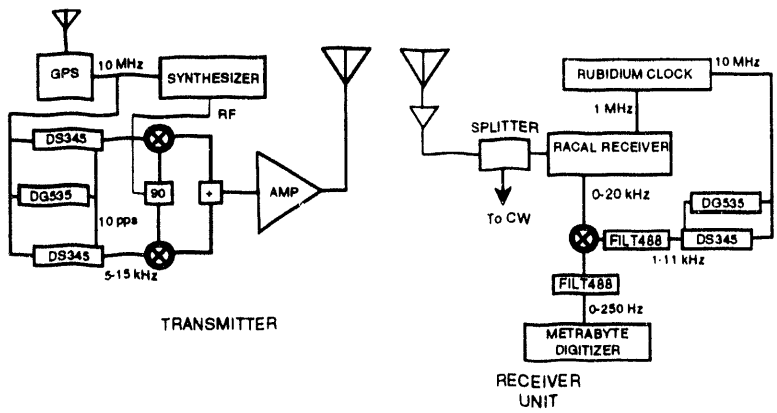

Figure 3: Diagram of the channel probe transmitter and receiver system.

from sweep to sweep. Differences in the sweep rates of the two synthesizers affect the individual ionogram; the performance of the system is satisfactory for our purposes. The only problem that arose was one hour of data collection when the GPS system at the receive site lost lock on satellites. Curiously, this was during one of the periods during which severe Spread F effects observed: 2300-2400, Jan. 14 (EST).

2.3 Channel Probe System

The channel probe is designed to obtained time delay and Doppler information; it is also designed to be easily extensible to obtain the same data simultaneously from a number of spatially separate antennas. In addition, it was designed to also to obtain the same information from an OTH radar using the same waveform. In a sense the channel probe gives a combination of the information obtainable from the oblique ionogram and the cw systems. However, unlike the ionogram it is limited to one frequency. The channel probe is essentially an fmcw radar with highly separated transmitter and receiver stations. As with the oblique ionogram, a linear frequency sweep is used at both ends to obtain time delay via the frequency offset. But the frequency range for the channel probe is much smaller while the repetition rate is higher to obtain Doppler information. For our experiment we used a sweep rate of 100 kHz/s and a repetition rate of 10 Hz giving a bandwidth of 10 kHz. The same parameters were used by the AVA radar. Figure 2 shows a block diagram of the transmit and receive portions of the channel probe system. Table 3 lists the operational frequencies for the channel probe system; during the one hour time period, 2200-2300 EST on Jan. 14, we changed frequencies in 1 MHz steps every 15 minutes.

Unlike the oblique ionogram we do not generate the sweep directly from a synthesizer but mix an audio sweep with an rf tone from a synthesizer. In order to measure Doppler, the transmitted waveform must be coherent from sweep to sweep. We achieve that by using a Stanford Research Systems DS345 Synthesized Function Generator; the DS345 can store a digitized sweep waveform and output it when properly triggered. At the transmitter we use a DS345 to store 15,900 points of a waveform that begins with a frequency of 5 kHz and

Day (EST)	Time (EST)					
	1800	1900	2000	2100	2200	2300
Jan 10			10.91	9.41	9.41	9.41
Jan 11	11.41	10.91	10.91	9.41	9.41	9.41
Jan 12	11.41	10.91	10.91	9.41	9.41	9.41
Jan 13	11.41	10.91	10.91	12.91	12.91	12.91
Jan 14	13.41	12.91	12.91	multi	10.91	10.91

Table 3: Channel probe frequency in MHz.

sweeps at 100 kHz/s; the waveform is output at a rate of 160 kHz so that the sweep lasts 99.4 ms. We trigger the DS345 at a 10 Hz rate using a Stanford Research Systems DG535 digital delay generator; the DG535 and the DS345 are locked to the 10 MHz reference from a GPS receiver. Using this external reference, the 10 Hz trigger rate generated internally by the DG535 is stable to less than 500 ns.

If we simply mixed the audio sweep and the rf our transmitted signal would contain power at the carrier frequency as well as in both sidebands. We suppress the carrier and the lower sideband by using a technique adapted from single sideband radio. We use a second DS345 to generate a waveform 90° out of phase to the first; we generate a second rf signal using a passive 90° splitter. When these are properly mixed and summed the lower sideband is suppressed by about 40 dB and the carrier somewhat more.

The receiver side of the channel probe is not completely complementary to the transmitter side because we use a Racal receiver with 20 kHz bandwidth to select the upper sideband and suppress the lower sideband. That is, the rf from the antenna preamplifier is input into a receiver that is tuned in cw mode so that the upper sideband in our case comes out as a sweep from 1 to 11 kHz. The Racal receivers usually have 7 and 20 kHz bandwidths but not a 10 kHz. This audio output is mixed with a corresponding sweep from a DS345 triggered in the same manner as at the transmitter end. We use the DS535 to adjust the delay so that the mixed signals fall in the 0-250 Hz range. After low pass filtering the mixed signal is digitized at a 500 Hz rate.

One advantage to the fmcw technique is that one suppresses strong interferers in the band; the signal level is always relatively constant so that one can use the full range of the digitizer. An advantage of our technique is that one can change frequencies by simply changing one parameter on the synthesizer; a disadvantage is that we get incomplete suppression of the lower sideband. Again at the receiver end we can change frequencies by modifying one parameter. Using the receiver to suppress the lower sideband has the disadvantage that it introduces an uncalibrated delay into the system which varies with receiver bandwidth. It does appear that at least at 20 kHz bandwidth the Racal receivers are well matched.

Day (EST)	Time (EST)					
	1800	1900	2000	2100	2200	2300
Jan 10			6.81	6.81	6.81	6.81
Jan 11	6.81	6.81	6.81	6.81	6.81	6.81
Jan 12	6.81	6.81	6.81	6.81	6.81	6.81
Jan 13	6.81	6.81	6.81	9.11	9.11	9.11
Jan 14	9.11	9.11	9.11	9.11	9.11	9.11

Table 4: AVA frequency in MHz.

2.4 AVA One-Way Propagation

The waveform of the AVA radar transmission was the same as that of our channel probe system; we could therefore use one component of our channel probe system to monitor the AVA transmission. We had planned to use a second DS345 audio synthesizer triggered independently from the second channel of the D535 delay generator to mix with the received waveform. Unfortunately, the second DS345 was unreliable; we therefore had to use the same DS345 for both the channel probe and the AVA components. The two transmissions were synchronized to the even second so that because of its longer path the AVA transmission arrived at about 17 ms delay relative to the arrival of the channel probe transmission. That delay corresponds to a frequency offset of 1700 Hz which was well outside our desired passband of 250 Hz; to shift the audio frequency into our passband we offset the tuning of the AVA receiver. That has the effect of reducing the time period of usable data in each sweep or effectively the bandwidth of the transmission by about 2 kHz. In retrospect, we could have compensated for the difference in delay by offsetting the channel probe timing by 17 ms so that the received chirps began at the same time for both the channel probe and the AVA transmissions. Table 4 lists the AVA frequencies during the experiment.

2.5 Antenna Geometry

We deployed four antennas normal to Piura-Arequipa path; we had a fifth antenna for the oblique ionogram system. These antennas were magnetic loops about 1 m in diameter; there output was amplified by 30 dB and fed through a cable to the receiver building. The closest spacing was 38 m while the greatest was 316 m. For most of the data we used only the three closest antennas for the channel probe and the fourth antenna for the AVA channel.

2.6 Problems

We encountered a number of difficulties but not as many as we had anticipated. We had a series of power problems at Arequipa which ate up time during the set up. The temperatures at Piura were very high during the daytime making activity difficult; the air conditioner was not able to keep the container that housed our transmitters cool. Splatter from our

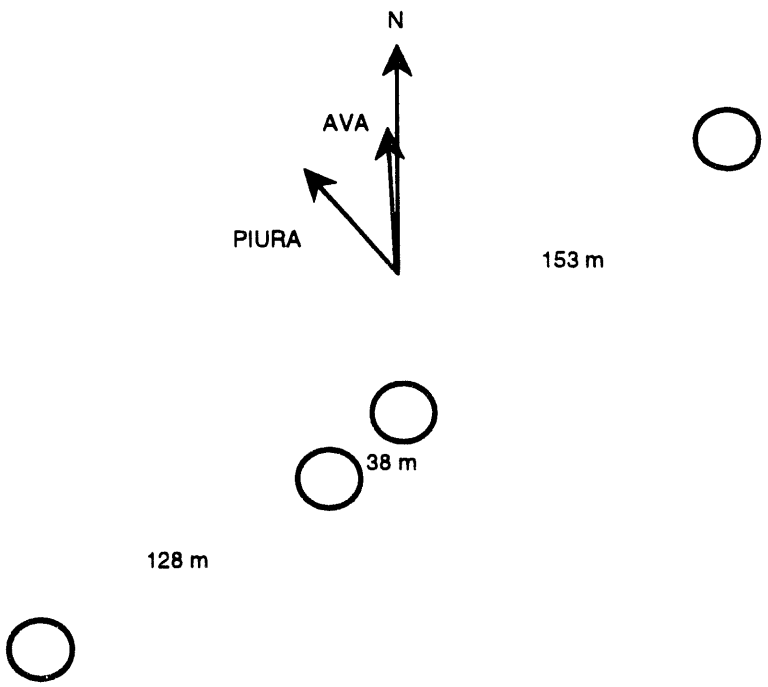

Figure 4: Diagram of the spatial orientation of the receiver antennas.

transmitters, particularly the oblique sounder, interfered with the 50 MHz wind profiler at Piura. We tried to avoid being on the air during their operational period. Telephone communications presented some difficulties. The receiver site at Arequipa seemed to be in a poor location for cellular service so that connections were often noisy or weak or nonexistent. The switchboard at the University of Piura was closed after 7:00PM so that the transmitter site could not receive calls. Long distance lines in Peru also have limited availability at some times of day. We were able to coordinate frequencies with AVA before each day's run; we did at least once change frequencies during the run without problems.

We encountered considerable difficulty in getting the channel probe to work for eight channels using one DS345. Our solution was to use four channels of the FILT488 filter module as a splitter and low-pass filter for the output of the DS345; we then had the other four channels available to use as a low pass filter for the mixer at the output of the receivers. We divided the four available channels into three for the channel probe and one for the AVA radar.

A number of problems that we had worried about did not materialize. The University of Piura expedited the transfer of our equipment through customs very efficiently. We also had considerable support at our sites. Each site employed two assistants who were very helpful and at least one was fluent in English. The Peruvian Air Force Base at Arequipa afforded us enough secure space to set out our antenna array. Security at both sites was good.

3 Results.

To give an impression of the types of data obtained during the experiment we will show the results of the data set obtained between 1837 and 2000 EST on Jan. 14, (2337 to 0100 UT Jan. 14/15). During this time period the ionosphere developed significant bottomside Spread F which affected both the Piura-Arequipa and the AVA-Arequipa paths.

3.1 Oblique Ionograms

Figure 5 shows two successive ionogram sweeps beginning at 2342 UT obtained by plotting the power spectrum of the mixed signal according the the color scale depicted; the abscissa shows time in seconds while the ordinate shows the frequency of the mixed signal in Hz. The first sweep begins at 0 s while the second begins at 180 s. The ordinate, f, may be converted to time delay in milliseconds, τ, using the conversion $\tau = (450 + f)/90.9$ which includes factors for the frequency offset and the sweep rate. Thus the ordinate scale in Figure 5 includes about 1 ms of delay beginning at 5.6 ms. The intense peak between 60 and 100 Hz represents the one-hop reflection and shows no resolvable broadening; there is a separation of o and x modes particularly at lower frequencies. The peak continues up to our maximum sounding frequency (20 MHz) so that we do no see the typical muf behavior of a full ionogram. At low frequencies, there are indications of a spread two-hop F mode at $\tau \approx 6.5$ ms and a spread two-hop mixed $(E - F)$ mode at $\tau \approx 6.1$ ms. Figure 6 shows two successive ionograms obtained one hour after those shown in Figure 5; in the interim Spread F had developed and delay spread had affected all the observable frequencies. There was also a significant increase in total delay accompanying the rise of the ionosphere during this period; we estimate from this data that the average vertical drift was 38 m/s.

3.2 CW Doppler Spectra

From the CW data we are able to get information on the Doppler spreading that occurred on the Piura–Arequipa path. Figure 7 shows the time behavior of the Doppler spectra of the cw transmission for one element of the array plotted according to accompanying power scale. The spectra were calculated from 12.8 s of data every 9 s. The abscissa is the time in seconds after 2342 UT; the ordinate is the Doppler shift relative to the cw carrier frequency. The transmission frequency was initially 13.37 MHz; it was changed to 12.87 MHz at 2400 UT or 1080 s on the time scale in Figure 7. Initially the spectra show an intense peak near -0.5 Hz corresponding to the one-hop mode. There is also a weaker and broader peak near -1.5 Hz which we ascribe to the two-hop mode; the broadening is likely to have arisen from time variations of the scatter in the mountainous topography near the midpath. The digisonde data indicates that the critical frequency was about 10.5 MHz so that two-hop would propagate but that three-hop would be marginal. The negative displacement of the Doppler increased with time indicating an acceleration in the rise of the ionosphere. At about 1900 s or 0014 UT the one-hop mode started to broaden and became increasingly broad for the rest of the data set while the Doppler shift decreased. The increase in spectral power near +10 Hz is an alias artifact introduced in the analysis of the reduced sample rate

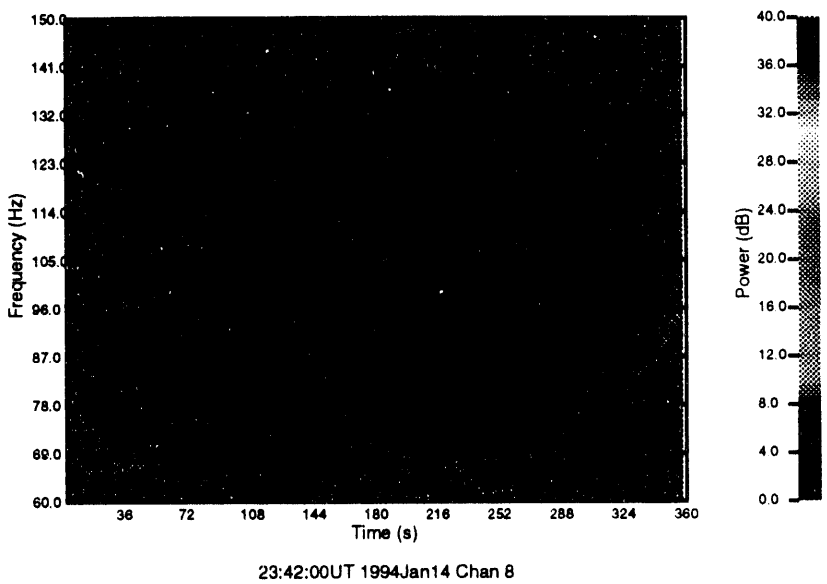

Figure 5: Power spectra versus time for the oblique ionogram between Piura and Arequipa beginning at 2342 UT, Jan. 14. The ordinate, f, may be converted to time delay in milliseconds, τ, using $\tau = (450 + f)/90.9$. The frequency sweep lasted 176 s and began at 4 MHz and ended at 20 MHz; the sweep was repeated starting at 180 s.

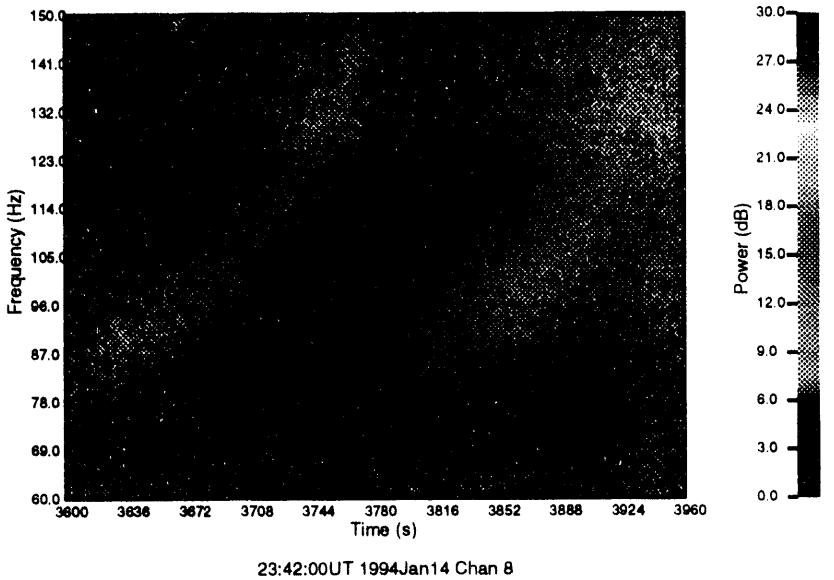

Figure 6: Oblique ionograms obtained one hour after those shown in Figure 5; the formats are the same. The Spread F that had developed during the interim produced delay spread at all the frequencies observed.

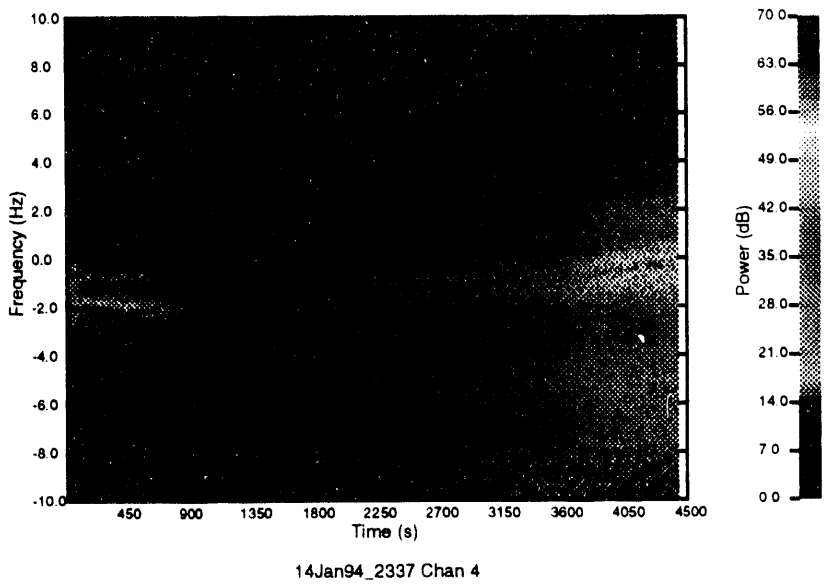

Figure 7: Time history of the power spectra of the cw transmission between Piura and Arequipa beginning at 2342 UT on Jan. 14. Doppler broadening caused by Spread F onset after 1900 s.

data and would not appear in spectra calculated from the original data. Figure 8 shows the received power versus time corresponding to the data in Figure 7; there is a distinct change in fading rate after 1900 s even with the 12.8 s window used in the analysis.

3.3 CW Spatial Coherence

We may characterize the spatial correlation of the cw signals from the separate antennas by calculating the coherence, γ; the coherence of two time series, x and y, as a function of frequency, f, is defined as

$$\gamma_{xy}^2(f) = \frac{|S_{xy}(f)|^2}{S_x(f)S_y(f)} \tag{1}$$

where S_x and S_y are the power spectra of x and y and S_{xy} is the cross power spectrum [*Otnes and Enochson*, 1978]. The coherence may be interpreted as a correlation coefficient in the frequency domain [*Priestley*, 1981]. In our case the frequency, f, is the Doppler offset; the coherence has the advantage that it will resolve the one and two hop modes which are otherwise mixed in the time domain. One can calculate the spectra from sampled data using the usual techniques but to get a reliable estimate of the coherence one must perform some averaging in the frequency domain. *Beningnus* [1969] suggested dividing the time series

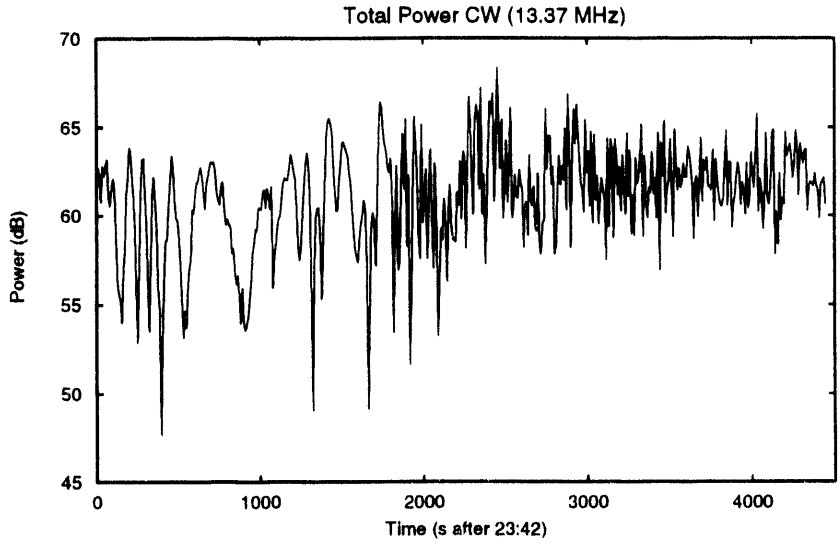

Figure 8: Time history of the total received power of the cw transmission between Piura and Arequipa beginning at 2342 UT on Jan. 14. Spread F onset after 1900 s led to an increased fading rate.

into m segments, calculating the Fourier transform and power spectra in each segment, and then averaging the results for the various segments. Thus

$$\bar{\gamma}^2_{xy}(f) = \frac{|\bar{S}_{xy}(f)|^2}{\bar{S}_x(f)\bar{S}_y(f)} \tag{2}$$

where

$$\bar{S}_{xy}(f) = \sum^{m} S_{xy}(f) \tag{3}$$

$$\bar{S}_x(f) = \sum^{m} S_x(f). \tag{4}$$

The statistics of $\bar{\gamma}^2_{xy}$ depend upon how much averaging is done but in general the estimate has a bias which depends on the value of $\bar{\gamma}^2_{xy}$. ***Beningnus*** [1969] developed an unbiased estimate, $\tilde{\gamma}^2_{xy}$,

$$\tilde{\gamma}^2_{xy} = \bar{\gamma}^2_{xy} - \hat{B}(\bar{\gamma}^2_{xy}) \tag{5}$$

where the bias, $\hat{B}(\bar{\gamma}^2_{xy})$, is given by

$$\hat{B}(\bar{\gamma}^2_{xy}) = \frac{1}{m}(1 - \bar{\gamma}^2_{xy}). \tag{6}$$

Figure 9 shows $\tilde{\gamma}^2_{xy}$ versus time for cw data from the antennas spaced 38 m apart. This calculation was made from 51.2 s of data divided into four segments; the frequency resolution is the same as that in Figure 7. Initially the one-hop mode had a coherence near unity

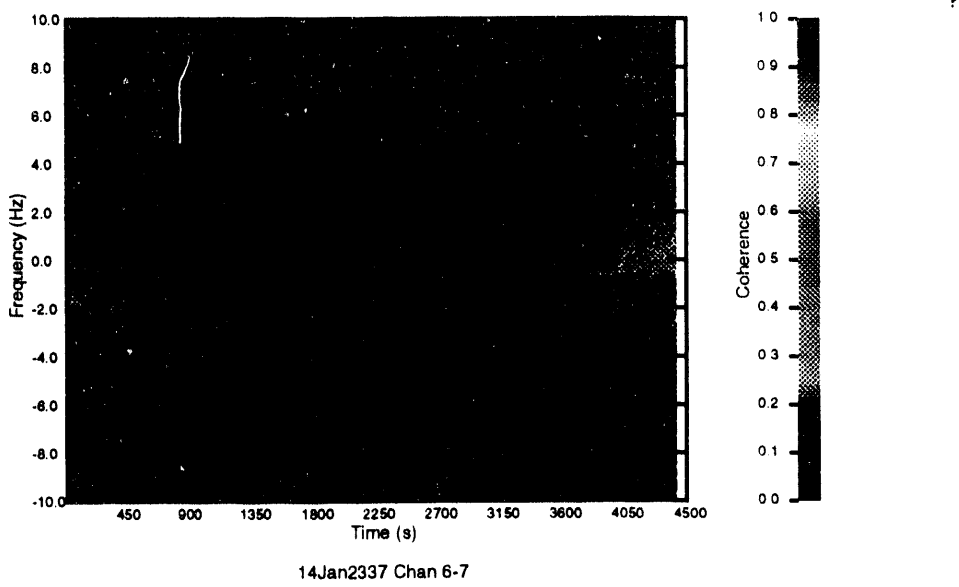

Figure 9: Time history of the coherence of the cw transmission between Piura and Arequipa beginning at 2342 UT on Jan. 14 for the two antennas spaced 38 m apart. Spread F onset after 1900 s led to a decreased coherence.

while the two-hop had a lower value and was spread. The cw frequency change at 1080 s was marked by a brief broadening. The onset of Spread F was marked by a broadening and decrease of the coherence for the one-hop mode and a null value for the two-hop mode.

3.4 Channel Probe Time Delay

The channel probe signals can be analyzed using either a double or single Fourier transform method to obtain time delay and Doppler information [*Barrick*, 1971]. The crude time delay behavior can be obtained using a low resolution (short time series) Fourier analysis. Figure 10 shows increased time delay spread after the onset of Spread F at 1900 s for the time period described above. The abscissa shows time in seconds after 2342 UT while the ordinate shows the frequency of the mixed signal in Hz; since the sweep rate was 100 kHz/s, the ordinate corresponds to a total time delay of 2.5 ms. The two-hop mode was initially also present in this data; there was a carrier frequency change at about 1080 s.

3.5 Channel Probe Doppler Spectra

If the channel probe signals are analyzed at increased resolution one resolves the delay bins and obtains the Doppler behavior versus delay. Figure 11 shows the behavior of the Doppler

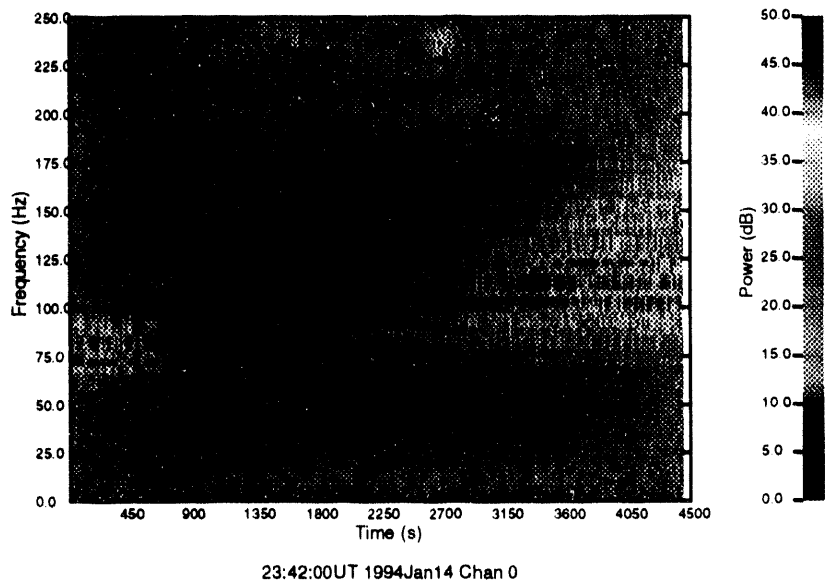

Figure 10: Time history of the time delay behavior of the channel probe transmission between Piura and Arequipa beginning at 2342 UT on Jan. 14. Spread F onset after 1900 s led to an increased delay spread.

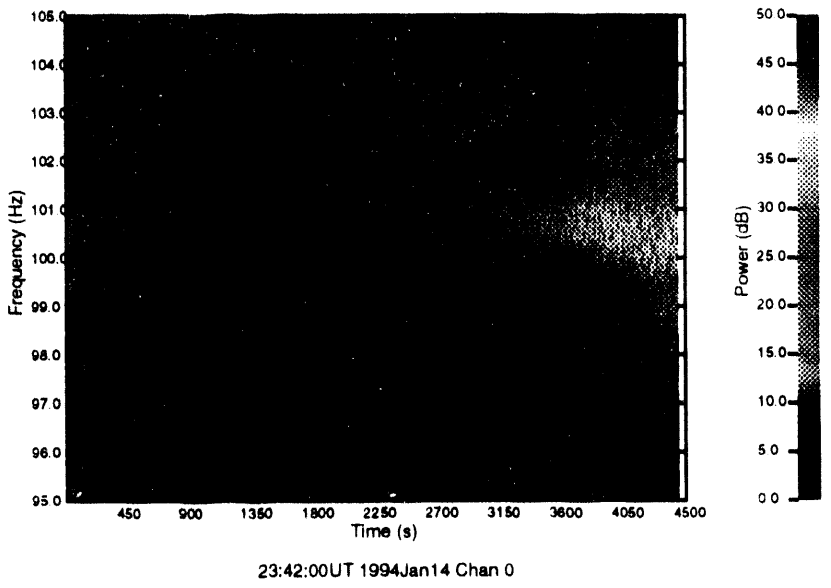

Figure 11: Time history of the Doppler behavior of the channel probe transmission between Piura and Arequipa beginning at 2342 UT on Jan. 14. Spread F onset after 1900 s led to an increased Doppler spread.

versus time delay for the delay centered at 100 Hz; the ordinate is the Doppler offset in Hz where zero Doppler is 100 Hz. The Doppler shift is reversed from the usual convention employed for the cw data. There is also weak artifact peak at the negative Doppler shift of the main peak. The Doppler spread is enhanced after the onset of Spread F.

3.6 Channel Probe Spatial Coherence

The spatial coherence of the channel probe signals from different antennas may be determined in the same manner as for the cw signals. Figure 12 shows the coherence of the channel probe signals at a single delay bin (100 Hz) versus Doppler offset for the time period beginning at 2342UT. The antennas correspond to those used for the cw coherence shown in 9; the results are similar but Figure 12 does not show the two-hop contribution but does show coherence in the artifact peak.

3.7 AVA Time Delay

The time delay structure of the AVA signal recorded at Arequipa can be obtained in the same manner as for the channel probe data. Figure 13 shows the results for the time period

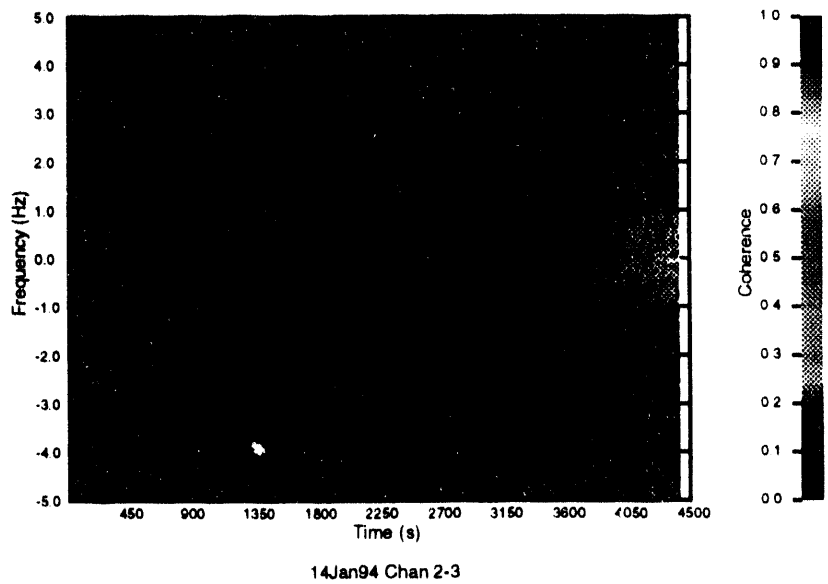

Figure 12: Coherence of the channel probe signals between two antennas spaced 38 m apart versus time beginning at 2342 UT on Jan. 14. Spread F onset after 1900 s led to a decrease in coherence.

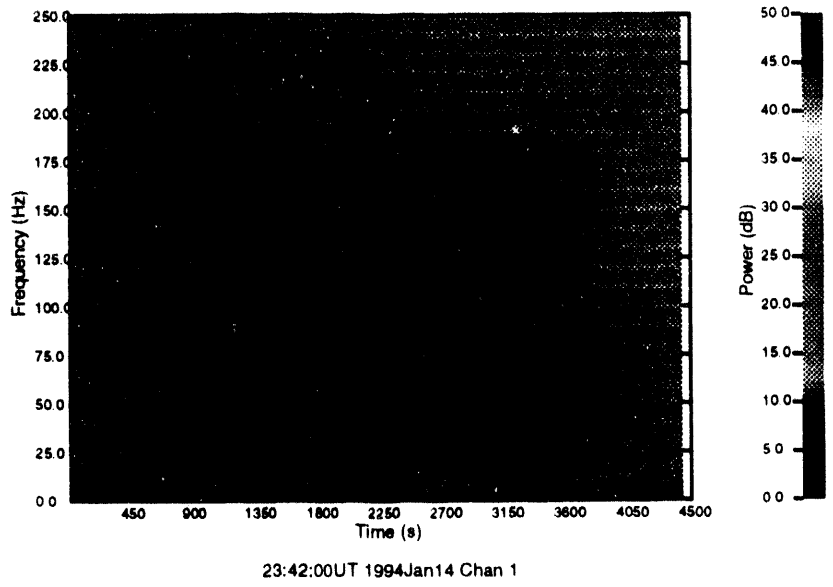

Figure 13: Nested time delay plot of the AVA signal received at Arequipa beginning at 2342 UT on Jan. 14. The ordinate corresponds to 2.5 ms of delay; even before the onset of spread the path showed more than 2.5 ms of delay spread.

beginning at 2342 UT. We note that even in quiet ionospheric conditions the signal was spread over more than the 2.5 ms of delay shown. The effect of Spread F was chiefly apparent in the Doppler spread.

3.8 AVA Doppler Spectra

The Doppler spread of the AVA transmission received at Arequipa for the delay associated with a frequency of 100 Hz is shown in Figure 14 for the time period beginning at 2342 UT. The analysis is the same as that used for the channel probe data shown in Figure 11: the ordinate is Doppler frequency where zero Doppler corresponds to 100 Hz. It is likely that the sign of the Doppler is reversed from the usual convention for this data also. The path initially shows a negative Doppler apparently imposed by the rising ionosphere near the equator; there is increased Doppler spread after 2000 s similar to that observed on the one-hop equatorial path. The simultaneous occurrence of spread on both the Piura–Arequipa and AVA–Arequipa paths indicates the influence of the equatorial ionospheric reflection in controlling the amount of Doppler spread observed.

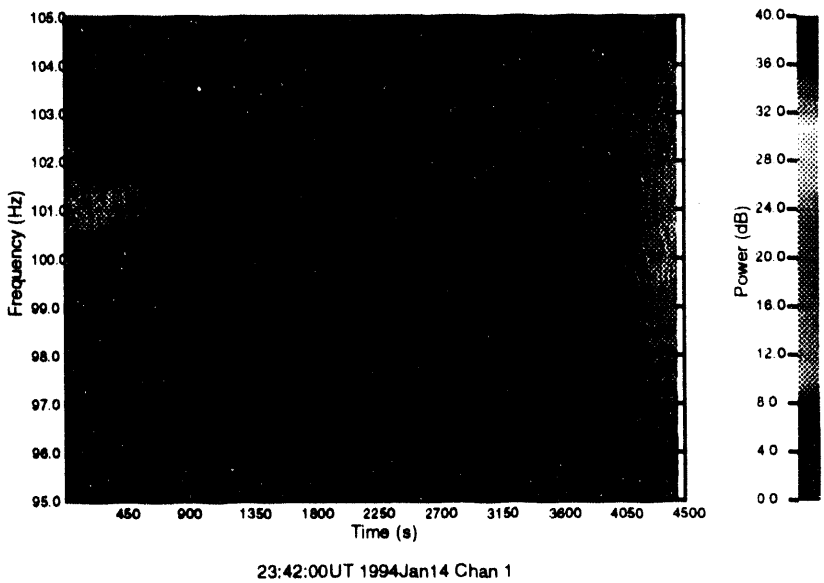

Figure 14: Doppler spread of the AVA signal received at Arequipa beginning at 2342 UT on Jan. 14 for the delay centered at 100 Hz. There was enhanced Doppler spread after 2000 s similar to that observed on the Piura–Arequipa path.

4 Conclusions.

We obtained a unique set of data consisting of time-delay, Doppler spread, and spatial coherence over a hf path across the geomagnetic equator together with a simultaneous transmission from the an OTH radar located at a range of 6700 km. We collect 26 hours of data using our channel probe system of which 15 hours showed Spread F effects. Simultaneous data from the Jicamarca 50 MHz radar are available for 9 hours of the Spread F period; 11.5 hours of simultaneous data during the Spread F period are available from the Jicamarca digisonde. In this report we presented an analysis of about one hour's worth of our data showing the transition to Spread F conditions. The time period analyzed is only a small and not particularly representative segment of our data; later time periods on the evening of Jan. 14 show even greater Doppler spreads. Further analysis of our data would enhance our understanding of the effects of Spread F on hf transmissions.

5 Acknowledgement

This work was funded by the U. S. Air Force, Rome Laboratories, and performed under the auspices of the U. S. Department of Energy by Los Alamos National Laboratory under contract W-7405-ENG-36. Bill Spurgeon of Los Alamos National Laboratory was invaluable in many phases of the experiment particularly as Station Manager at Piura. Dr. Carlos Calderon of the Jicamarca Observatory was of great assistance in expediting the logistics of the experiment. Ms. Maricarmen Avalos of the University of Piura handled the customs and forwarding with great efficiency. Srs. Renzo Forlin, Pablo Ortiz, and Rodolfo Rodriguez were very helpful in the execution of the experiment and serving as translators.

6 References

Barrick, D. E., *FM/CW Radar Signals and Digital Processing, Tech. Rept. ERL 283-WPL 26*, National Oceanic and Atmospheric Administration, Boulder, CO, July, 1973.

Beningnus, V. A., Estimation of the coherence spectrum and its confidence interval using the fast Fourier transform, *IEEE Trans. Audio and Electroacoustics, AU-17*, 145–150, 1969. Wiley, New York, 1978.

Otnes, R. K. and L. Enochson, *Applied Time Series Analysis*, Wiley, New York, 1978.

Priestley, M. B., *Spectral Analysis and Time Series*, Academic Press, San Diego, 1981.

DATE
FILMED
7/5/94
END